Optimal Speed Planning using Limited Preview for Connected Vehicles with Diesel Engines

C. Huang, R. Salehi, T. Ersal & A.G. Stefanopoulou
Department of Mechanical Engineering
University of Michigan, Ann Arbor, MI, United States

Speed planning in a vehicle-following scenario can reduce vehicle fuel consumption even under limited traffic preview and in moderate penetration of connected autonomous vehicles (CAVs), but could also lead to colder exhaust temperature, and consequently, less efficient aftertreatment conversion. To investigate this potential trade-off, this paper presents a model predictive controller (MPC) to optimally plan in an energy-conscious way the optimal speed trajectory for a diesel car following a hypothetical lead vehicle that drives through the velocity trace of a federal test procedure. Using this energy-conscious optimal speed plan we investigate different horizons for three objective functions, including minimum acceleration, minimum fuel consumption and minimum power. Then, MPC results are compared to the trajectories obtained by dynamic programming with full knowledge of the drive cycle. As expected, longer previews lead to smoother velocity trajectories that reduce the fuel consumption by 11% when power is the objective function, if the preview is accurate. When the minimum fuel is set as the objective in the MPC, the controller coordinates to operate the engine at more efficient conditions, which increases the fuel saving to 25%. However, the extra fuel saving is shown to be achieved at the expense of high vehicle NOx emissions, since the engine operates at low speeds and high loads, where the output NOx emissions are high, when the aftertreatment catalyst is not hot enough. Finally, it is shown that the minimum power formulation leads to a better trade-off, where fuel economy can be increased without a large penalty on NOx emissions.

1 INTRODUCTION

Speed planning has high potential for improving the fuel economy of a connected autonomous vehicle (CAV) by adjusting the vehicle speed for the given traffic and road conditions. When speed planning is performed in a car following scenario, traffic information is transmitted to the CAV through vehicle-to-vehicle (V2V) or vehicle-to-infrastructure (V2I) communication, and the CAV can utilize this information to predict its future driving environment and optimize its speed trajectory to guarantee safety while improving fuel economy.

Over the past decade, there has been extensive research on CAV speed planning for better fuel economy. The authors in [14] summarized and quantified possible energy reduction benefits brought by vehicle connectivity and autonomy, including reducing air drag loss, smoothing acceleration and deceleration, avoiding stoppage or powertrain downsizing. An algorithm that can realize these benefits is not included in [14], however, examples can be found in [1, 8, 10]. In particular, the effect of air drag reduction was experimentally studied in [1] and it was shown that for conventional vehicles, following the front vehicle closely and reducing air drag friction is an effective way to save fuel. To avoid stopping at traffic lights, traffic signal prediction is used in [8] with deterministic dynamic programming in a receding horizon manner. The effect of reduced acceleration and deceleration on improving fuel efficiency was demonstrated in [10], where the controller was tested on an Advanced Light-Duty Powertrain and Hybrid Analysis Tool using different drive cycles.

The effect of engine operation optimization, which is not considered in the above-mentioned studies, is included in e.g. [2, 4, 12, 5] in addition to reducing trip energy demand as researchers aim at minimizing fuel consumption under different scenarios. Specifically, a look-ahead road grade information is used in [2] to improve fuel efficiency for a heavy-duty vehicle platoon when traveling uphill and downhill, and initiating the change in velocity at a specific point in the road, rather than accelerating simultaneously with the lead vehicle, is shown to be the most fuel efficient strategy. For a single heavy-duty vehicle, an optimal speed planning framework with information of road elevation, headwind, desired terminal time and traffic is proposed in another effort, to design a fuel economy optimized trajectory, where the engine runs on pre-selected most efficient gear levels [4]. A scenario where two succeeding vehicles with following distance constraints is considered in [12]. In particular, by assuming a fixed gear level and approximating fuel consumption map with a convex piecewise linear function, the authors show that this controller outperforms a simple PI distance tracking controller in saving fuel while satisfying certain distance constraints. In the study reported in [5], fuel efficiency is optimized for a CAV as it is following a lead vehicle driving a known trip through dynamic programming.

Vehicle emissions also depend on the driving style as, e.g., a sudden acceleration may create a spike in the engine out emissions, which will lead to large tailpipe emissions if the aftertreatment system is not efficient enough. However, the above-mentioned studies did not consider the emissions with fuel economy simultaneously. Hybrid electric vehicles can mitigate the trade-off between fuel efficiency and tailpipe emissions by managing the torque split ratio between combustion engines and electric motors to balance fuel consumption and emissions [6, 15]. For conventional vehicles, there could be a severe trade-off between minimizing the fuel consumption by smoothing accelerations and maintaining the aftertreatment to the optimum temperature range. Two single objective optimizations, namely fuel optimal or emission optimal trajectory assuming perfect knowledge of the whole trip, result in more emissions or fuel consumption compared to the non-optimized trip [5]. Engine raw emissions can be reduced if high pedal positions are penalized during real-time speed planning [11], but as aftertreatment temperature drops due to reduced energy and torque demand, the overall change in tailpipe NOx is hard to predict.

Although integration of the powertrain information into the speed planning controller is important to realize the advantage of fuel saving by autonomy and connectivity as suggested in [12], it is not clear how much benefit can be gained through engine operation point optimization or lost due to the simplification in the objective function, e.g. from fuel consumption to acceleration as is used in [10] and [8]. To fill in this gap, this paper investigates the effect of the objective function and prediction horizon

when a model predictive controller is used in a car-following scenario to design the speed trajectory of a CAV with a conventional diesel engine powertrain. Three different objective functions, including minimum acceleration, minimum fuel consumption and minimum power, are studied for optimization, while constraints are applied to maintain a reasonable driving distance to ensure safety and tracking. Emission performance out of the three different objectives under different horizons are also discussed. As the first contribution of this paper, a detailed analysis of visitation points of the engine is presented to show how the engine speed and torque distribution changes with selection of the objective function. As a second novel contribution, it is shown that despite the noticeable fuel economy advantage, the direct fuel consumption optimization increases the vehicle NOx emissions; thus, it does not stand out as the best objective function for speed planning in the context of this work. Instead, vehicle power optimization is observed to create a better balance between fuel minimization and emissions.

The remaining part of this paper is organized as follows. In Section 2, a following vehicle model is developed to capture the longitudinal dynamics, fuel consumption and tailpipe (TP) NOx emissions. Section 3 defines the speed planning problem as an optimal control problem, and explains the MPC implementation. Section 4 shows the simulation results, and discusses about the effect of optimization objective and prediction horizon on fuel consumption and emissions performance. Finally, Section 5 concludes the paper.

2 VEHICLE MODEL

2.1 Vehicle longitudinal dynamics

Assuming the vehicle as a point mass, the states of the system $[v, p_{\text{veh}}]^T$, i.e. the vehicle velocity and position or distance from the starting point, satisfy:

$$\begin{bmatrix} p_{\text{veh}}(k+1) \\ v(k+1) \end{bmatrix} = \begin{bmatrix} 1 & T_s \\ 0 & 1 \end{bmatrix} \begin{bmatrix} p_{\text{veh}}(k) \\ v(k) \end{bmatrix} + \begin{bmatrix} 0.5T_s^2 \\ T_s \end{bmatrix} a(k), \quad (1)$$

in which a is the vehicle acceleration input, and T_s is the sampling time, which is chosen as 0.1s in this paper. Constant acceleration is assumed during each sampling period.

To calculate the fuel consumption, the following model is developed for a MY2013 Ford F-350 Super-duty truck with a 6.7L diesel engine. The vehicle is subjected to air drag f_{air}, rolling resistance f_{rr} and vehicle driving force f_D:

$$f_D = M_{\text{veh}} a + f_{rr} + f_{\text{air}} \quad (2)$$

$$f_{\text{rr}} = C_R M_{\text{veh}} g, \text{ if } v > 0 \quad (3)$$

$$f_{\text{air}} = 0.5 \rho_{\text{air}} A_f C_d v^2, \quad (4)$$

with f_{rr} being the rolling resistance, f_{air} the air drag resistance, M_v vehicle mass, A_f the vehicle frontal area, C_d and ρ_{air} the air drag coefficient and density, and C_R the rolling resistance coefficient.

Then, the demanded power PW_D for driving the vehicle at each step is calculated as:

$$PW_D(k) = f_D v. \quad (5)$$

2.2 Engine model

To simplify the model for optimization, we used data from a medium duty truck running a federal test procedure (FTP) to construct an empirical gear level lookup table for each vehicle speed and acceleration.

Then, the engine speed N_e and torque T_q are calculated from v and f_D using the gear shifting logic, and by assuming a constant drive-line efficiency of 75%. As a result, $N_e(k)$ and $T_q(k)$ are directly determined by $v(k)$ and $a(k)$ using (6,7):

$$N_e(k) = \frac{60}{2\pi R_w} F_R G_R v(k) \quad (6)$$

$$T_q(k) = \frac{f_D v(k)}{0.75 N_e(k)} \quad (7)$$

with F_R as the final drive ratio, G_R as the gear ratio and R_w as the wheel radius.

Engine outputs including fuel consumption $\dot{m}_{\text{fuel}}$, NOx emissions $\dot{m}_{\text{Eng.NOx}}$, exhaust mass flow rate $\dot{m}_{\text{exh}}$ and exhaust upstream temperature T_{eu} are calculated using lookup tables depending on engine speed and torque calibrated based on engine dynamometer test data. As an example, Fig. 1 shows the relative fuel rate at different vehicle speed and acceleration. Validation results of the engine speed N_e, torque T_q and fuel rate $\dot{m}_{\text{fuel}}$ are shown in Fig. 2. As shown, the modeled engine torque and fuel rate in Fig. 2-(c),(d) approximates measured data quite well, except that it predicts higher oscillations during transient conditions. One reason for these oscillations is that the model does not include the torque converter, which could damp out the engine speed and torque oscillations. Engine speed in Fig. 2-(b) is mostly captured, but some error occurs because of the mismatch of the gear level.

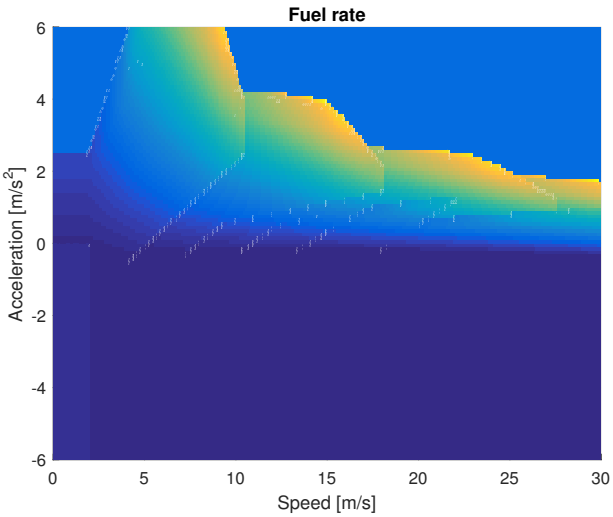

Figure 1: Lookup table for relative fuel rate based on vehicle speed and acceleration by assuming a fixed gear shifting logic

2.3 Thermal dynamics and emissions model

The aftertreatment system includes a diesel oxidization catalyst (DOC) and a selective catalytic reduction (SCR) system. A turbine (TB) is located on the downstream of the engine and on the upstream of the DOC. It is assumed that engine NOx emission is only reduced in the SCR catalyst once it is emitted out of the engine. As the SCR conversion efficiency is dependent on the catalyst brick temperature, a thermal model for the aftertreatment system together with the turbine is needed to calculate tailpipe NOx emissions.

A first order lag is assumed for turbine outlet gas temperature, $T_{g.\text{TB}}$, dynamics:

$$T_{\text{g.TB}} = \frac{1}{1+\tau s} T_{\text{eu}} \quad (8)$$

where the time constant τ is assumed to be inversely proportional to exhaust mass flow rate $\dot{m}_{\text{exh}}$.

Due to the similarities in DOC and SCR catalysts' structures, the DOC and SCR catalysts are both modeled as thermal masses, and their gas and brick temperatures are calculated by (9) and (10) [7]:

$$T_{g.i} = \frac{\frac{\dot{m}_{\text{exh}} C_{pg}}{(A\Delta x)_i} T_{\text{in}_{\text{delay}}.i} + (h_1 a_1)_i T_{b.i}}{(h_1 a_1)_i + \frac{\dot{m}_{\text{exh}} C_{pg}}{(A\Delta x)_i}} \quad (9)$$

$$(1-\epsilon_i)\rho_b C_b \frac{dT_{b.i}}{dt} = (h_1 a_1)_i (T_{g.i} - T_{b.i}) - (h_2 a_2)_i (T_{b.i} - T_a) \quad (10)$$

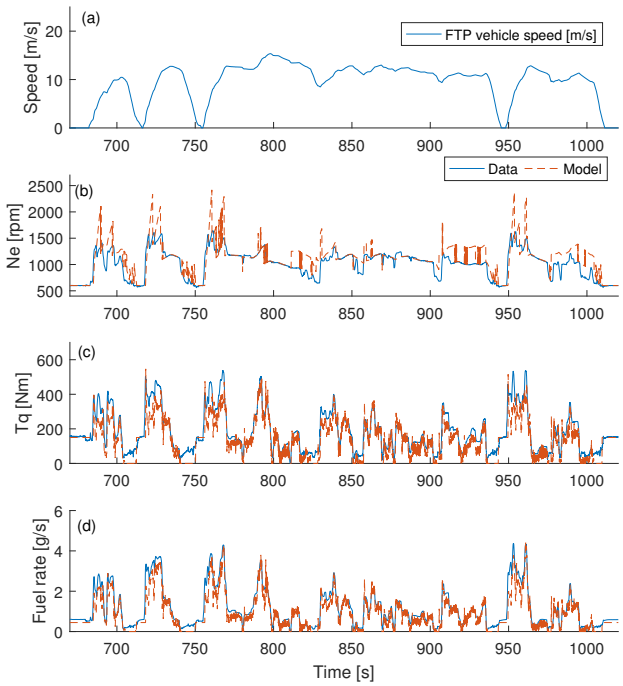

Figure 2: Validation results for vehicle longitudinal dynamics and fuel rate

in which $i = \{\text{DOC}, \text{SCR}\}$, T_b, T_g are brick temperature and gas temperature, T_a is the ambient temperature. A, Δx and ρ_b are the frontal area, length and density of the brick, C_{pg} and C_b are the specific heat capacities of the exhaust gas and monolith, ϵ is the parameter showing the fraction of the catalyst brick open cross sectional area, h_1 and h_2 are the heat convection coefficient from the gas flow to the monoliths, and from the brick surfaces to the ambient, a_1 and a_2, are the corresponding geometric surface area-to-volume ratios [9].

The input to (9), $T_{\text{in}_{\text{delay}}.i}$, is calculated as [5]:

$$T_{\text{in}_{\text{delay}}.i}(t) = T_{g\text{in}.i}(t - \Delta\tau_{d.i}) \tag{11}$$

$$\int_{t-\Delta\tau_{d.i}}^{t} \dot{m}_{\text{exh}} ds = l_{d.i}, \tag{12}$$

where $T_{g\text{in.DOC}} = T_{g.TB}$, $T_{g\text{in.SCR}} = T_{g.\text{DOC}}$.

Once $T_{b.\text{SCR}}$ is known, NOx reaction efficiency η is determined by a lookup table [3], and thus the tailpipe NOx emission $\dot{m}_{\text{TP.NOx}}$ can be modeled as:

$$\dot{m}_{\text{TP.NOx}} = \eta(T_{b.\text{SCR}})\dot{m}_{\text{Eng.NOx}}. \tag{13}$$

Validation results of the SCR temperature are shown in Fig. 3. An underestimation is shown to happen in Bag1 of FTP trajectory, as the effect of the engine post-fuel injection warming up the aftertreatment system is not included in this thermal model. After the warm-up phase of Bag1, the SCR catalyst temperature is predicted with a maximum error of 14% and average error of 4%. This error is deemed sufficiently low, because, for the purpose of this work, the thermal dynamics is used to explore the temperature variations when speed trajectory changes.

3 MODEL PREDICTIVE CONTROL

We consider the scenario that a CAV is following another connected vehicle, which is driving a federal test procedure. In order to explore the benefit of connectivity and autonomy, instead of letting the autonomous vehicle to exactly follow its leader vehicle's trajectory or track the leader's position strictly, we pose a spacing constraint on the following distance to mimic the traffic

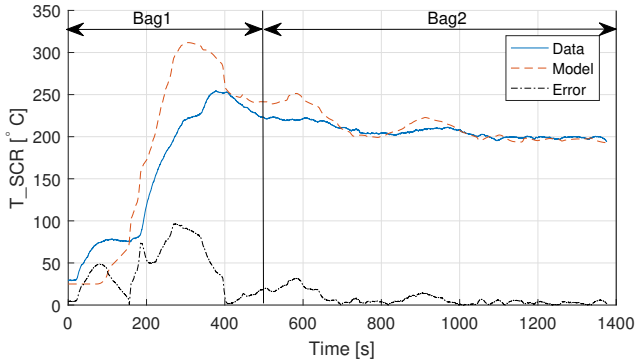

Figure 3: Validation results for the SCR temperature calculated using aftertreatment thermal dynamics

constraints to avoid rear end collisions and keep the following distance from being too long to avoid frequent cut-ins from adjacent lanes. Any following trajectories that satisfy this spacing constraint are considered feasible. Then, the velocity trajectory of the following vehicle can be optimized to reduce fuel consumption.

Three candidate functions as separate minimization objectives are chosen, including acceleration, power and fuel consumption. For each of the three considerations, the cost function at every step k over a horizon of N_P steps is expressed as:

$$J_i(k) = \sum_{j=0}^{N_P-1} C_i(k|j), i = \{1, 2, 3\} \tag{14}$$

and Table 1 lists the objective functions of each case.

Table 1: Cost functions defined for all optimization scenarios

i	Case	Objective to minimize	Cost function
1	MPC_a	acceleration	$C_1(k\|j) = a(k\|j)^2$
2	MPC_p	power	$C_2(k\|j) = \|PW_D(k\|j)\|$
3	MPC_f	fuel	$C_3(k\|j) = m_{\text{fuel}}(k\|j)$

Braking and tractive power are both penalized. Tractive power obviously increases fuel consumption. Reduction of braking power also decreases fuel consumption since traveling the same distance at the same time with less braking would incur less friction losses that do not allow all the kinetic energy to be recuperated [1].

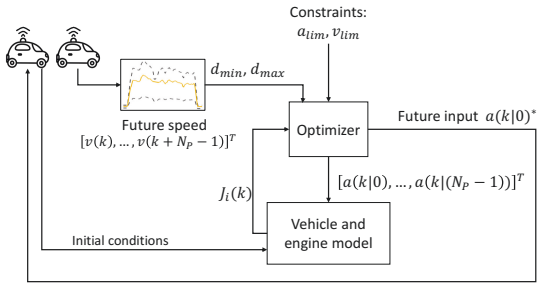

Figure 4: Architecture of the implemented MPC algorithm

In Table 1, $a(k|j)$, $PW_D(k|j)$ and $m_{\text{fuel}}(k|j)$ refer to the predicted value of a, PW_D and m_{fuel} at step $k+j$ while current step is denoted with k, and N_P in (14) is the prediction horizon of the model predictive controller. The prediction horizon in terms of time is given as $T_P = N_P \cdot T_s$. The structure of the controller is shown in Fig. 4. The controller determines the optimization variable U, which collects the future inputs in the vector: $U = [a(k|0) \quad a(k|1) \quad \cdots \quad a(k|(N_P-1))]^T$, by minimizing the cost function over the prediction horizon N_P while

[1] Penalization of braking power should also be applied even if regenerative braking, as in hybrid vehicles, would be possible.

utilizing future speed of the leading vehicle and system dynamics, and accounting for the input and state constraints. The spacing constraint of maximum and minimum admissible following distances, d_{max} and d_{min}, are two piece-wise linear functions of the lead vehicle speed v_l [5, 10]. Here we assume accurate preview velocity of the lead vehicle is known within the prediction horizon, so its position p_l can be calculated. Then the following vehicle's position p_{veh} should satisfy:

$$\begin{cases} p_{\text{veh}}(k) \leq max(p_l(k) - d_{min}(v_l(k)), p_{\text{IC}}) \\ p_{\text{veh}}(k) \geq max(p_l(k) - d_{max}(v_l(k)), p_{\text{IC}}) \end{cases}, \tag{15}$$

where

$$d_{min}(v_l) = 0.3v_l \tag{16}$$

$$d_{max}(v_l) = \begin{cases} 4v_l - 3 & \text{if } v_l \geq 20 \text{ MPH} \\ 10v_l - 3 & \text{if } v_l < 20 \text{ MPH} \end{cases} \tag{17}$$

and $p_{\text{IC}} \geq 0$ is the initial distance between the two vehicles, and is assumed to be 10m.

Other motion constraints are imposed to the vehicle speed and acceleration. Considering the maximum possible power of the vehicle and driver comfort, the vehicle acceleration is constrained by:

$$-6\text{m/s}^2 \leq a(k) \leq 6\text{m/s}^2, \tag{18}$$

where the maximum acceleration and deceleration are chosen twice of that of the standard FTP drive cycle, and vehicle velocity is constrained by:

$$0\text{m/s} \leq v(k) \leq 30\text{m/s}, \tag{19}$$

which is very close to the typical highway speed limit in the USA.

Satisfying (18) and (19) does not guarantee sufficient engine power, as, for example, the power demand for achieving 3m/s^2 acceleration at 5m/s speed is different from that at 25m/s. So for speed and acceleration points that satisfy (18) and (19) but require higher power than the engine maximum, the corresponding cost function value is set to $+\infty$ to avoid infeasible operating conditions.

To summarize, the controller solves for the optimal decision variable U of the following problem:

$$\min_{U} \quad J_i(k) \tag{20}$$

Subject to

$$\begin{bmatrix} p_{\text{veh}}(k|j+1) \\ v(k|j+1) \end{bmatrix} = \begin{bmatrix} 1 & T_s \\ 0 & 1 \end{bmatrix} \begin{bmatrix} p_{\text{veh}}(k|j) \\ v(k|j) \end{bmatrix} + \begin{bmatrix} 0.5T_s^2 \\ T_s \end{bmatrix} a(k|j)) \tag{21}$$

$$\begin{bmatrix} 1 & 0 & 0 \\ -1 & 0 & 0 \\ 0 & 1 & 0 \\ 0 & -1 & 0 \\ 0 & 0 & 1 \\ 0 & 0 & -1 \end{bmatrix} \begin{bmatrix} p_{\text{veh}}(k|j+1) \\ v(k|j+1) \\ a(k|j) \end{bmatrix}$$

$$\leq \begin{bmatrix} max(p_l(k+j+1) - d_{min}(v_l(k+j+1)), p_{\text{IC}}) \\ -max(p_l(k+j+1) - d_{max}(v_l(k+j+1)), p_{\text{IC}}) \\ 30 \\ 0 \\ 6 \\ 6 \end{bmatrix} \tag{22}$$

where $j = \{0, 1, ..., N_p - 1\}$.

The above optimization problem is solved using the fmincon command available in the MATLAB optimization toolbox. Then the optimized input at current step k is implemented and the controller proceeds to optimize for the next step until the end of the trajectory. The MPC is not fast enough yet to finish solving the optimization problem at each step within $T_s = 0.1$s, but the investigation of increasing computation speed is subject to a future study.

4 SIMULATION RESULTS AND DISCUSSIONS

The vehicle speed calculated by the MPC over Bag2 of the Federal Test Procedure for heavy duty vehicles is presented in Fig. 5 for different prediction horizons T_P and for fuel consumption minimization MPC_f. Also, global optimal results form Dynamic Programming [13, 5] (DP) and a conventional driving style emulated by a PI driver model tracking FTP are included to evaluate the MPC performance. The driver model is a PI feedback controller developed based on system dynamics (1) to track vehicle speed, with maximum tracking error smaller than $\pm$1mph. As plotted in Fig. 5-(a),(b), a longer prediction horizon $T_P = 24$s yields a smoother speed trajectory and smaller distance between the two vehicles compared to a shorter prediction horizon of 6s. As plotted in Fig. 5-(c), the trajectory from the 6s-horizon controller stays close to the maximum following distance. This is because the controller with a shorter horizon does not ask for acceleration until the following vehicle moves very close to highest distance constraint. Thus the final speed trajectory has more oscillations, with corresponding oscillations in the engine speed and load.

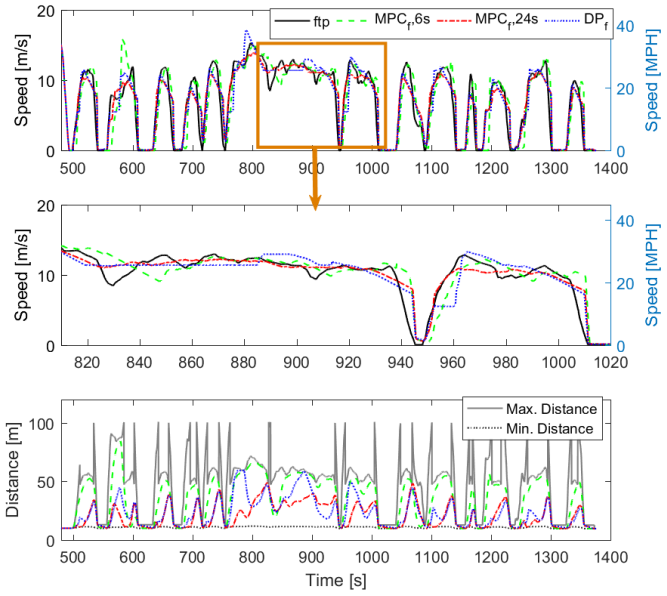

Figure 5: Prediction horizon affects driving pattern in MPC_f

The effect of the prediction horizon on the controller performance is shown in Fig. 6. As shown in Fig. 6-(c), when the prediction horizon is as long as $T_P = 26$s, with MPC_f, the vehicle fuel economy is improved by 25% compared to the PI driver model, very close to the global optimal fuel consumption result of DP. Average engine efficiency achieved by MPC_f is not as high as DP in Fig. 6-(d). This is expected as DP guarantees global minimum solution, while MPC only returns locally minimum results. MPC_P also approaches DP result in terms of the objective function value as is observed in Fig. 6-(a). Both MPC_a and MPC_p controllers show a potential of reducing the fuel consumption by 7% and 11%, respectively, with a with $T_P = 26$s prediction horizon. It is worth noting that the short horizon controllers may not be able to generate a feasible input that satisfies both the input constraint (18) and the distance constraint (15) because of the limited reaction time. In the simulations, when $T_P < 6$s, with MPC_a and MPC_f controllers, upper distance bound violations were observed with a maximum of 6m, in addition to their poor fuel efficiency results.

The speed trajectory optimization reduces the energy required for driving the vehicle as shown in Fig. 6-(a), and at the same time, the energy wasted by braking is reduced (Fig. 6-(b)). As shown, minimizing either fuel consumption or power, i.e. MPC_f and MPC_p, reduces the required energy to the same order, but more than the energy reduction obtained by minimizing the ac-

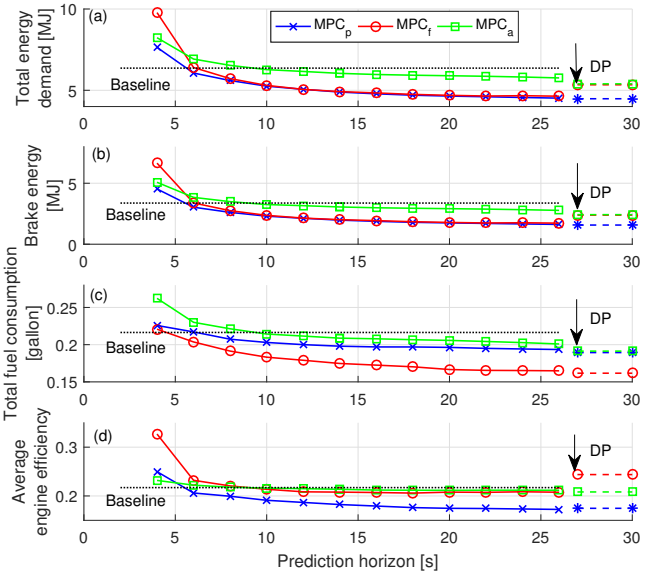

Figure 6: Effect of objective function and prediction horizon on (a) trip energy demand (b) trip brake energy (c) trip fuel consumption and (d) average engine efficiency

celeration with MPC_a. However, the vehicle trip total fuel usage is shown to be reduced more with MPC_f, 14% more with a 26s prediction horizon compared to MPC_p (Fig. 6-(b)). This indicates the importance of explicit inclusion of the engine fuel efficiency model in the optimization problem, since MPC_f trajectory has a cycle averaged engine efficiency of 21% compared to 17% obtained with MPC_p (Fig. 6-(d)). This causes the MPC_f with $T_P = 8$s to be more fuel efficient than MPC_a or MPC_p with the long horizon of $T_P = 26$s.

Another important observation shown in Fig. 6-(c) is that the engine efficiency decreases with increased prediction horizon. This happens because with increased prediction, the required vehicle energy and consequently the engine power reduces. For internal combustion engines, lower power (or torque assuming a constant speed) operating conditions are less efficient. This can be seen in their engine operation visitation. Figure 7 shows the engine visitation points for (MPC_a, $T_P = 12$s), (MPC_p, $T_P = 6$s) and (MPC_f, $T_P = 6$s) trajectories. These three trajectories have similar drive energy demand: 6.2MJ for MPC_a, 6.1MJ for MPC_p, and 6.4MJ for MPC_f. By looking at the engine visitation plots of these three cases, the effect of engine operation optimization can be seen. As is shown by the colorbar, the more time is spent, the darker the color is. Comparing Fig. 7-(c) with Fig. 7-(a),(b), MPC_f spends the highest amount of time visiting low BSFC (brake specific fuel consumption) region, and thus has the highest fuel efficiency.

Cycle averaged NOx emission results are shown in Fig. 8 for different controllers and prediction horizons. As Fig. 8-(a) shows, the engine out NOx emissions reduce when the prediction horizon increases, since the engine operates at lower power and torque conditions. As a consequence of the lower power and torque operation of the engine, the lower bound of the simulated SCR temperature reduces with increased horizon (Fig. 8-(b)). A comparison between SCR temperature traces of FTP trajectory, MPC_f controller with $T_P = 6$s, 24s and DP result as shown in Fig. 9 also indicates that SCR temperature reduces with increased horizon. The SCR temperature reduction decreases the catalyst NOx conversion efficiency plotted in Fig. 8-(c). For MPC_a and MPC_p, the decrease in the SCR efficiency is mitigated by the reduction in the engine out NOx, such that the total tailpipe emissions remains almost constant with increasing horizon. However, with MPC_f, the engine NOx will be higher than MPC_p (Fig. 8-(a)) despite their similar energy demand and similar SCR temperature. This is because the MPC_f coordinates the engine to operate at lower speed but higher torque points, where engine NOx emission is high. As a result, MPC_f leads to much more tailpipe emissions compared to MPC_a and MPC_p, and the total tailpipe NOx emission increases as prediction horizon increases (due to lower SCR temperature and efficiency). For all the simulated prediction horizons, the vehicle with MPC_f emits significantly more tailpipe NOx emissions than the PI-model driven standard FTP drive cycle. When the speed trajectory is selected from the MPC_p controller, however, a 9% fuel saving is achieved with prediction horizon $T_P \geq 16$s, with tailpipe NOx emissions similar to the baseline FTP simulations. Thus, MPC_p controller with $T_P \geq 16$s stands out as a better choice for the CAV speed planning studied in this work.

5 CONCLUSIONS

The influence of different predictive speed controller designs and prediction horizon on the performance of a CAV driven in a car-following scenario on the Federal Test Procedure has been presented. Controllers with three different objective functions including fuel consumption, demanded power, and acceleration have been tested with prediction horizons between 4s and 26s. Results show that even under limited preview, model predictive controllers with 26s prediction horizon achieves fuel consumption results that are within 5% of the dynamic programming results, where perfect knowledge of the entire prediction horizon is assumed. Results also show that with the same objective function, longer prediction horizons save more fuel. Furthermore, direct inclusion of the engine fuel consumption map in the optimization achieve the most fuel saving (25%) among the three case studies, since it both optimizes engine operation and reduces trajectory energy demand. These fuel efficiency benefits come with the stark realization that better fuel economy pushes the engine to run at lower speed and higher load region, where the raw engine NOx emissions increase. Compounding the adverse influence on tailpipe emissions, the velocity smoothing enabled by the connectivity leads to colder aftertreatment, and consequently, less efficient emissions reduction for a fixed (size and catalyst loading) aftertreatment system.

The results point to the need for an even more complex optimization process that includes the full fuel and emission models in the optimizer. This complex optimization problem could be addressed in the future. Meanwhile, the results in this paper highlight that reduction of the fuel consumption in the speed planning for a connected autonomous vehicle could lead to higher real driving emissions (RDE) if the trade-off is not carefully considered.

ACKNOWLEDGMENTS

This material is based upon work supported by the National Science Foundation under Grant No. 1646019. The authors would like to thank Michiel Van Nieuwstadt and Cory Hendrickson from Ford Research and Advanced Engineering for providing valuable data and suggestions regarding constructing the model.

REFERENCES

[1] Assad Al Alam et al. “An experimental study on the fuel reduction potential of heavy duty vehicle platooning”. In: *Intelligent Transportation Systems (ITSC), 2010 13th International IEEE Conference on*. IEEE. 2010, pp. 306–311.

[2] Assad Alam et al. “Look-ahead cruise control for heavy duty vehicle platooning”. In: *Intelligent Transportation Systems-(ITSC), 2013 16th International IEEE Conference on*. IEEE. 2013, pp. 928–935.

[3] Giovanni Cavataio et al. “Enhanced durability of a Cu/zeolite based SCR catalyst”. In: *SAE International Journal of Fuels and Lubricants* 1.2008-01-1025 (2008), pp. 477–487.

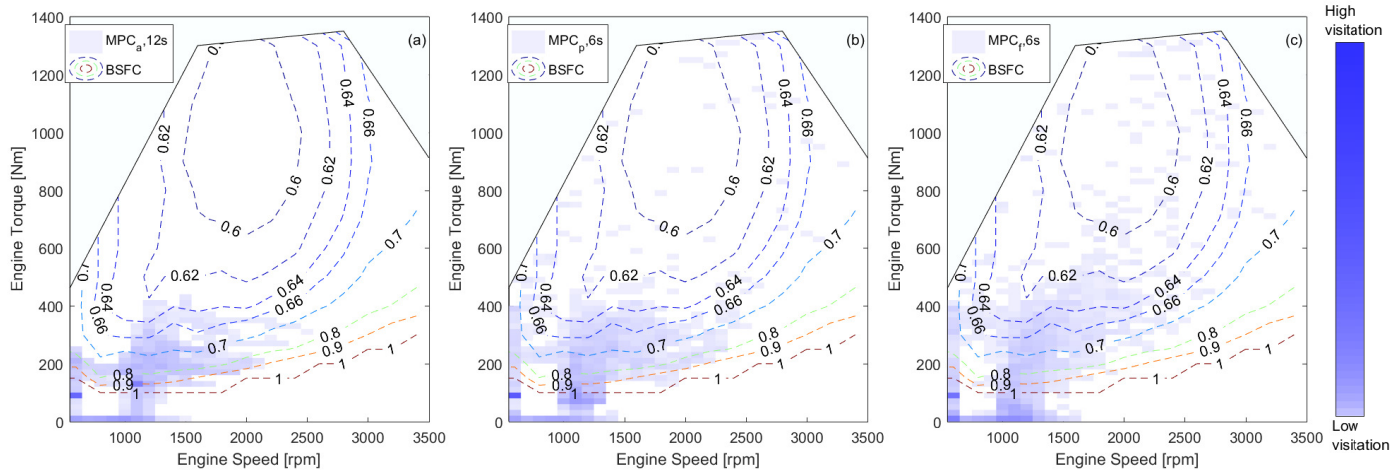

Figure 7: Engine operation condition of three trajectories with different objective functions. (a) MPC_a, $T_P = 12$s. Energy demand 6.2MJ, fuel consumption 0.212 gallon (b) MPC_p, $T_P = 6$s. Energy demand 6.1MJ, fuel consumption 0.217 gallon (c) MPC_f, $T_P = 6$s. Energy demand 6.4MJ, fuel consumption 0.204 gallon. BSFC curve is normalized to make the maximum value being 1 on the plot to show the relatively high and low efficiency regions

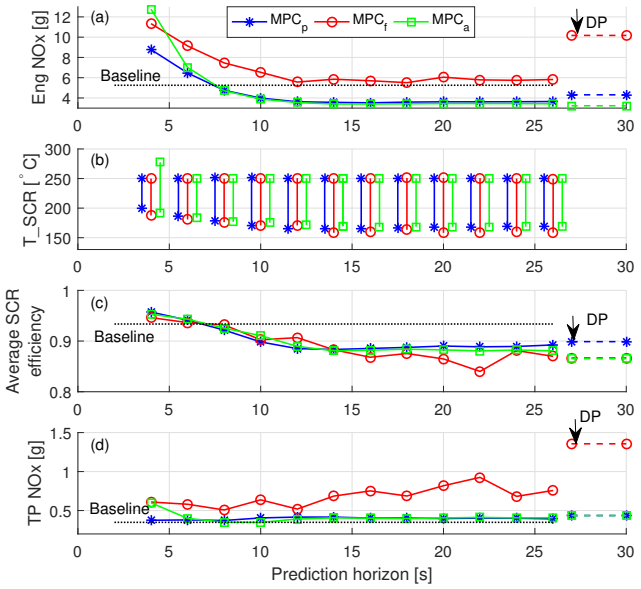

Figure 8: (a) Cycle averaged Engine NOx (b) Range of SCR temperature variation (c) Cycle averaged SCR efficiency (d) Cycle averaged tailpipe NOx emissions

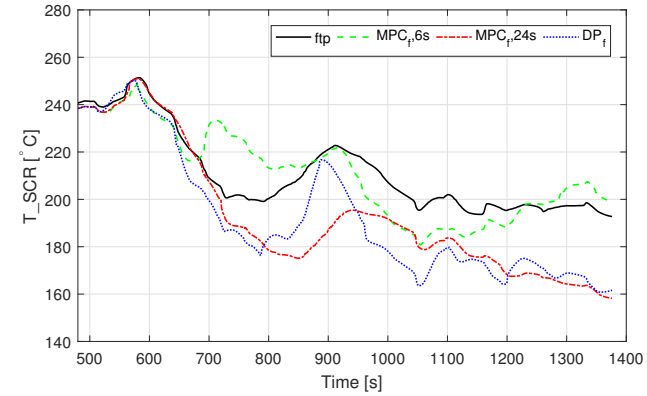

Figure 9: SCR temperature trace of different horizons using MPC_f compared with standard FTP cycle and DP result

[4] Chaozhe He et al. "Fuel consumption optimization of heavy-duty vehicles with grade, wind, and traffic information". In: *Journal of Computational and Nonlinear Dynamics* 11.6 (2016), p. 061011.

[5] Chunan Huang et al. "Intelligent Cruise Control of Diesel Powered Vehicles Addressing the Fuel Consumption Versus Emissions Trade-off". In: *American Control Conference (ACC), 2018*. IEEE. 2018, in press.

[6] Dongsuk Kum et al. "Optimal energy and catalyst temperature management of plug-in hybrid electric vehicles for minimum fuel consumption and tail-pipe emissions". In: *IEEE Transactions on Control Systems Technology* 21.1 (2013), pp. 14–26.

[7] Olivier Lepreux et al. "Model-based control design of a diesel oxidation catalyst". In: *IFAC Proceedings Volumes* 42.11 (2009), pp. 279–284.

[8] Grant Mahler et al. "An optimal velocity-planning scheme for vehicle energy efficiency through probabilistic prediction of traffic-signal timing". In: *IEEE Transactions on Intelligent Transportation Systems* 15.6 (2014), pp. 2516–2523.

[9] Varun Pandey et al. "A simplified thermal model for the three way catalytic converter". In: *TAP 2016, 21st International Transport and Air Pollution Conference*. 2016, 6 p.

[10] Niket Prakash et al. "Assessing Fuel Economy From Automated Driving: Influence of Preview and Velocity Constraints". In: *ASME 2016 Dynamic Systems and Control Conference*. ASME. 2016, V002T19A001–V002T19A001.

[11] Roman Schmied et al. "Nonlinear MPC for emission efficient cooperative adaptive cruise control". In: *IFAC-PapersOnLine* 48.23 (2015), pp. 160–165.

[12] Thomas Stanger et al. "A model predictive cooperative adaptive cruise control approach". In: *American Control Conference (ACC), 2013*. IEEE. 2013, pp. 1374–1379.

[13] Olle Sundstrom et al. "A generic dynamic programming Matlab function". In: *Control Applications,(CCA) & Intelligent Control,(ISIC)*. 2009, pp. 1625–1630.

[14] Louis Tate et al. "Energy Efficiency of Autonomous Car Powertrain". In: *SAE Technical Papers* 2018 (2018).

[15] Florian Tschopp et al. *Optimal Energy and Emission Management of a Diesel Hybrid Electric Vehicle Equipped with a Selective Catalytic Reduction System*. Tech. rep. 2015-24-2548. SAE, Warrendale, PA, 2015.